Tin Diselenide Molecular Precursor for Solution-Processable Thermoelectric Materials

Yu Zhang,[a] Yu Liu,[a] Khak Ho Lim,[b] Congcong Xing[a,c], Mengyao Li,[a] Ting Zhang,[d] Pengyi Tang,[d] Jordi Arbiol,[d,e] Jordi Llorca,[c] Ka Ming Ng,[b] Maria Ibañez,[f] Doris Cadavid,[g]* Andreu Cabot[a,e]*

Abstract: In the present work, we detail a fast and simple solution-based method to synthesize hexagonal nanoplates (NPLs) and their use to produce crystallographically textured $SnSe_2$ nanomaterials. We also demonstrate that the same strategy can be used to produce orthorhombic SnSe nanostructures and nanomaterials. NPLs are grown though a screw dislocation-driven mechanism with additional detachment of the growing layers, resulting in flower-like structures. $SnSe_2$ bulk nanomaterials with a significant crystallographic texture and obtained from the hot pressing of the $SnSe_2$ NPLs display highly anisotropic charge and heat transport properties. The overall thermoelectric (TE) figures of merit of thus obtained $SnSe_2$ nanomaterials is limited by their relatively low electrical conductivity. To improve this parameter, $SnSe_2$ NPLs are blended with metal nanoparticles. The electrical conductivities of the blends are significantly improved with respect to bare $SnSe_2$ NPLs and a three-fold increase in the TE figure of merit is obtained, reaching unprecedented values up to ZT = 0.65 for this material.

The use of molecular precursors to produce inorganic nanomaterials in the form of nanoparticles, thin films, supported nanostructures or self-standing porous or dense nanomaterials is potentially advantageous in terms of reducing fabrication costs and improving performances. In this direction, the amine-dithiol system has been reported as a versatile solvent to prepare molecular precursors from the dissolution at ambient conditions of metal chalcogenides, pure metals and metal oxides, among others.[1]

[a] Y. Zhang, Y. Liu, C. C. Xing, M. Y. Li, Prof. A. Cabot
Catalonia Energy Research Institute - IREC
Sant Adria de Besòs, 08930 Barcelona, Spain
E-mail: acabot@irec.cat
[b] K. H. Lim, Prof. K. M. Ng
Department of Chemical and Biological Engineering
Hong Kong University of Science and Technology, Hong Kong, China
[c] C. C. Xing, Prof. J. Llorca
Institute of Energy Technologies, department of Chemical Engineering and Barcelona Research Center in Multiscale Science and Engineering
Universitat Politècnica de Catalunya, 08019 Barcelona, Spain

Two dimensional (2D) materials have attracted increasing attention in the past decade. The structure of these materials is formed by atomically thin layers that display strong covalent in plane bonding and weak layer-to-layer bonding. This type of structure results in extraordinary physical, electronic and optical properties, but which are at the same time highly anisotropic. In particular, charge and heat transport properties are especially affected by the strong lattice asymmetry, resulting in much higher thermal and electronic conductivities in plane than cross plane. Owing to these highly anisotropic properties, to produce bulk 2D nanomaterials with a proper crystallographic texture is necessary to optimize their performance in most applications. However, to control the crystallographic texture of materials produced by bottom-up procedures and/or solution-based approaches is not straightforward.

A particularly interesting 2D material family is that of metal chalcogenides, owing to their good chemical stability and semiconducting characteristics. 2D metal chalcogenides are used in numerous applications in the fields of energy conversion and storage, [2] flexible electronics[3] and medical diagnosis[4]. Among them, tin chalcogenides are especially interesting materials for energy conversion. In particular, p-type SnSe have shown unprecedentedly high thermoelectric (TE) figure of merits (ZT): ZT = 2.6 at 923 K.[5] On the other hand, n-type $SnSe_2$ could be an ideal compound to complement an all Sn-Se based device, but the measurement of it TE properties and their optimization has been rarely targeted.[6]

Here we report on a fast solution-based methodology that makes use of molecular precursors to produce $SnSe_2$ nanoplates (NPLs) and $SnSe_2$ nanomaterials. The synthetic procedure can be easily scaled up, paving the way for commercial application. These NPLs are hot pressed to produce crystallographically textured nanomaterials, which TE properties are characterized. The final TE performance of $SnSe_2$ is further optimized through modulation doping by combining $SnSe_2$ NPLs with metal nanoparticles (NPs).

Tin diselenide NPs were produced through the thermal decomposition of an ink prepared by the dissolution of elemental Sn and Se powders with a Sn/Se=0.5 molar ratio in an amine-dithiol mixture (Figure S1, see experimental section for details). Upon heating of the ink to 380 ºC, the solvent was evaporated and a very rapid crystallization of tin diselenide NPs took place. This simple process could be carried out at virtually any scale and in a continuous manner, using a flow system, to produce very large amounts of material.

This procedure resulted in hexagonal plate-like NPs with average lateral sizes of ca. 500 nm and 70 nm thicknesses, as observed by TEM (Figure 1a). Such NPLs assembled into flower-like clusters with average size of ca. 4 µm (Figure 1b). XRD patterns of the obtained materials (Figure 1c) were consistent with a $SnSe_2$ crystal structure (P3-m1 space group, JCPDS NO. 01-089-2939). Along the z-axis of this structure, three-atom-thick and covalently bond Se-Sn-Se slabs were piled up together through weak van der Waals interaction (Figure 1d). The relatively strong intensity of the (001) XRD peak pointed at the [001] direction as the normal to the NPL plane. No additional phases were identified

by XRD. HRTEM analysis (Figure 1e) confirmed the $SnSe_2$ trigonal phase (space group = P3-m1) with a=b=3.8110 Å, c=6.1360 Å and the growth of the NPLs with preferentially exposed (001) facets.

Figure 1. (a) Representative TEM micrograph of a hexagonal $SnSe_2$ NPL. (b) Representative SEM micrograph of flower-like $SnSe_2$ nanostructures, including a magnified micrograph of an individual particle. (c) XRD pattern of $SnSe_2$ NPLs. (d) Atomic model of the $SnSe_2$ crystal structure (P3m1 space group) along Y and Z axis: Se (orange), Sn (light blue). (e) HRTEM micrograph, with magnified detail of the orange squared region and its corresponding power spectrum. The

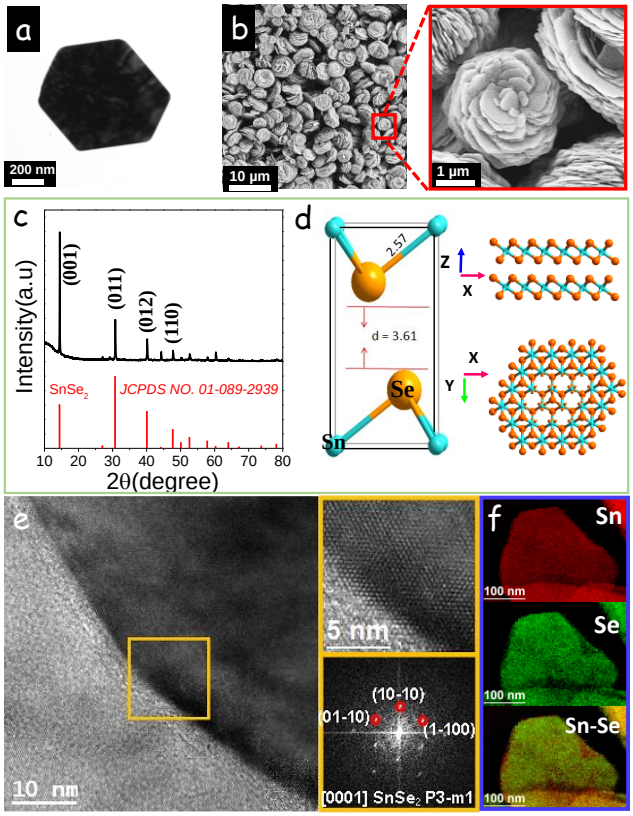

$SnSe_2$ lattice fringe distances were measured to be 0.332 nm, 0.327 nm and 0.326 nm, with crystal plane angles of 61.23 and 121.25º, which can be assigned to the trigonal $SnSe_2$ phase, visualized along its [0001] zone axis. (f) EELS chemical composition maps of $SnSe_2$ NPLs.

EDX analysis showed the $SnSe_2$ NPLs to be slightly Sn-rich, with a composition Se/Sn=1.9 (Figure S2). XPS analysis showed the surface of $SnSe_2$ NPLs to be slightly more Sn rich: Se/Sn = 1.7. The Se 3d and Sn 3d regions of the XPS spectra (Figure S3) could be fitted with a unique doublet each one, further proving the phase purity of the sample.[7] EELS chemical composition maps displayed a homogeneous distribution of both Sn and Se elements in all $SnSe_2$ NPLs (Figure 1f), although slightly Sn-rich edges could be detected.

SEM characterization displayed $SnSe_2$ NPLs to grow through a screw dislocation mechanism.[8] Figure 2b shows the top view and side view of a $SnSe_2$ multi-layer nanostructure displaying an helical surface on the top layer with clockwise spiral direction (Figure 2a, S4a). Bright field TEM micrographs of some of the NPLs also displayed multiple contours with different contrast (Figure S4c) also indicating screw dislocation phenomenon. In the screw dislocation growth mechanism self-perpetuating steps along a screw dislocation axis cause the oriental growth.[9] In contrast with several previous nanostructures obtained by the screw dislocation,[10] in our materials new $SnSe_2$ layers grown through the dislocation mechanism detached from previously formed, resulting in a flower-like structure (Figure 2b). We hypothesize the layer detachment resulted from the combination of the stress generated in nanostructures grown from such dislocation-driven mechanism and the weak layer-to-layer bonding in the 2D $SnSe_2$ crystal structure.

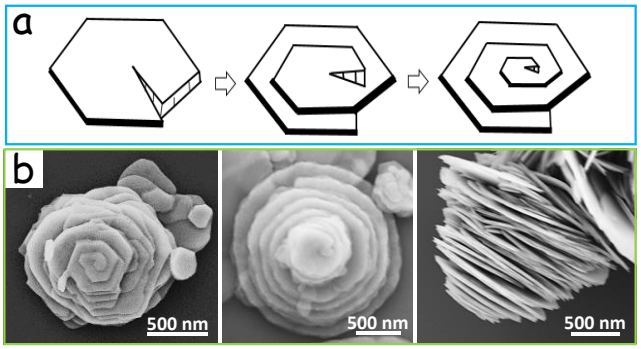

Figure 2. (a) Schematic illustration of the screw dislocation-driven growth mechanism. (b) Representative SEM micrographs of $SnSe_2$NPL-based structures revealing the screw dislocation growth from top view and side view.

The temperature and nominal molecular ratio of Sn and Se precursors were key parameters to produce phase pure $SnSe_2$ NPLs (Figure 3a). Sn/Se molar ratios above 0.5 in the initial ink resulted in the additional formation of a secondary SnSe phase. However, at Sn/Se=1 the ink decomposition at 380 ºC did not result in pure orthorhombic SnSe, but a combination of $SnSe_2$ and SnS_2 due to the reaction of part of the Sn with EDT. Pure-phase SnSe was obtained only at higher ink decomposition temperatures of ca. 500 °C and only when using equal concentrations of the two elements (Figure 3c).

$SnSe_2$ NPLs were purified by multiple precipitation and redispersion steps using chloroform as solvent and ethanol as antisolvent. The purified and dried NPLs were annealed at 450 °C for 60 mins inside a tube furnace under argon flow. The annealed particles still displayed plate-like geometries although with larger lateral dimensions and without displaying the flower-like shape (Figure 4a). We hypothesize the multiple layers of the initial NPL-based nanoflowers, combined within a unique plate, resulting in planar but larger nanostructures.

Subsequently, the annealed NPLs were loaded into a graphite die and were hot-pressed within an Ar-filled glovebox at 460 ºC for 5 min under 80 MPa of uniaxial pressure. This methodology allowed obtaining 10 × 10 (length × diameter) mm^2 cylinders with relative densities of ca. 90% as measured by Archimedes' method.

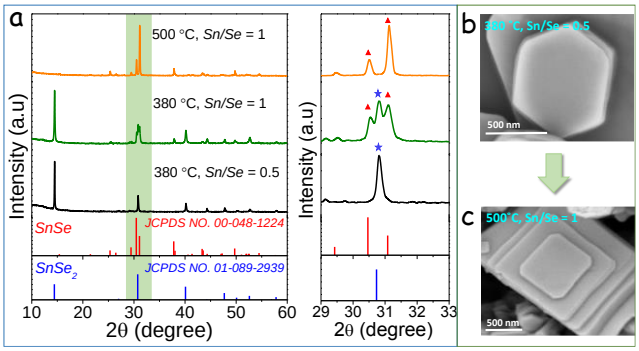

Figure 3. (a) XRD pattern of the material obtained from the decomposition of the precursor ink with different Sn/Se ratios and at different temperatures as specified in each pattern. A magnification of the relevant area around 2θ=31º is also shown for clarity. (b) SEM micrographs of $SnSe_2$ NPLs with hexagonal structure and (c) SnSe NPLs with orthorhombic nanostructure obtained in the specified conditions.

Such pellets, obtained from the uniaxial press of $SnSe_2$ NPLs, displayed a clear crystallographic texture, with the $SnSe_2$ [001] crystallographic direction oriented along the pressure axis, as observed from XRD characterization (Figure 4d). Top view and cross-section SEM micrographs displayed a clear laminar structure of the pellets (Figure 4b-c), with layers extending tens of microns in the disk plane and having a thickness of ca. 70 nm.

Such layered structure anticipated anisotropic transport properties. Thus, the TE properties of the material were measured in two normal directions: cross plane, which corresponds to the pressure axis and the [001] crystallographic direction, and in plane, which mainly corresponds to the ab plane of the $SnSe_2$ structure (Figure S5).

As expected, the electrical conductivities measured cross plane ($\sigma_\perp$), were lower than those measured in plane ($\sigma_{//}$): $\sigma_{//}/\sigma_\perp$ = 2.7 at 750 K. However, $SnSe_2$ nanomaterials exhibited relatively low electric conductivities in both measured directions (Figure 5a).

Negative Seebeck coefficients were obtained in all the temperature range (Figure 5b). The Seebeck coefficients displayed similar values in the two directions: $S_{//}/S_\perp$ = 0.91 at 750 K. These similar values are explained by the relatively low dependence of this parameter on scattering. Nevertheless, as generally observed in similar crystallographically textured layered nanomaterials, slightly higher values were obtained cross plane, which can be related to a slight preferential scattering of minoritarian and/or low energy carriers, i.e. a filtering mechanism.[11]

Much lower thermal conductivities were obtained cross plane than in plane: $\kappa_{//}/\kappa_\perp$ = 3.64 at 750 K (Figure 5d). This anisotropy was associated to the more efficient phonon scattering at the higher density of grain boundaries in the cross plane direction and the anharmonicity of the $SnSe_2$ crystal structure. In this regard, already in $SnSe_2$ single crystals highly anisotropic transport properties were generally measured, with electrical conductivity and thermal conductivity ratios up to 6 [12].

Overall, higher TE figures of merit were obtained cross plane, with values up to $ZT_\perp$=0.2 at 770 K (Figure 5f). These values were comparable to those previously measures for this material obtained by other methods.[6] Overall, while $SnSe_2$ nanomaterials displayed relatively high Seebeck coefficients and very low thermal conductivities, their main limitation was a moderate electrical conductivity. This low electrical conductivity was in part related to a moderate charge carrier concentration due to the lack of extrinsic dopants.

To increase electrical conductivity, instead of a conventional doping strategy, we used a modulation doping approach. While ionic doping generally relies on the introduction within a semiconductor matrix of small amounts of substituting impurities with different valence than the replaced element, thus freeing or trapping additional electrons, modulation doping relies on the introduction within a semiconductor matrix of nanodomains of a different material having an electron energy band structure suitable for injection of majority carriers to the matrix semiconductor.[13] The modulation doping approach allows separating the ionized donor/acceptor from the charge carrier path, thus strongly reducing charge carrier scattering and improving mobilities. Additionally, in NP-based bottom up assembly approaches, the modulation doping strategy provides a very simple and versatile strategy to optimize electrical properties of semiconductor materials,[14] since the charge injection nanodomains can be easily introduced in the proper amount during the assembly or consolidation steps.

Figure 4. (a) Schematic illustration of the consolidation the annealed

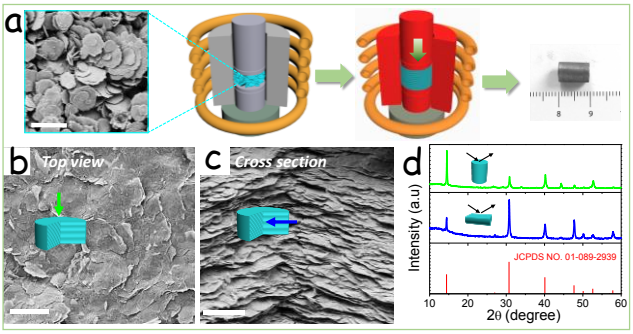

nanopowder into a cylindrical pellet. A representative SEM micrograph of the annealed nanopowder and an optical image of the final pellet are included in the scheme. (b) Top-view SEM micrograph of a $SnSe_2$ pellet. (c) Cross-section SEM micrograph of the same pellet. (d) XRD pattern of the $SnSe_2$ pellet laid along the cross plane direction (blue) and the in plane direction (green). Scale bar = 10 µm.

Being $SnSe_2$ an n-type semiconductor, we selected a dopant phase with a large charge carrier concentration and a relatively low work function that allowed injection of electrons to the $SnSe_2$ matrix. Thus, we blended $SnSe_2$ NPLs with Cu, Sn and Ag NPs (Figure 6a). While Sn had moderate effect on the transport properties of the material, upon incorporation of Cu or Ag NPs a dramatic increase in electric conductivity was measured (Figure S6a). As expected, a parallel decrease of the Seebeck coefficient was also obtained. This Seebeck coefficient decrease was more abrupt with the introduction of Ag NPs than with Cu. Overall, among the different metals tested, the highest power factors were obtained from $SnSe_2$-Cu nanocomposites (Figure S6c), reaching values three-fold higher than in pure $SnSe_2$.

We further studied the effect of the concentration of Cu NPs (Figure S7). We observed the electrical conductivity to increase with the amount of Cu introduced up to a certain loading. With the

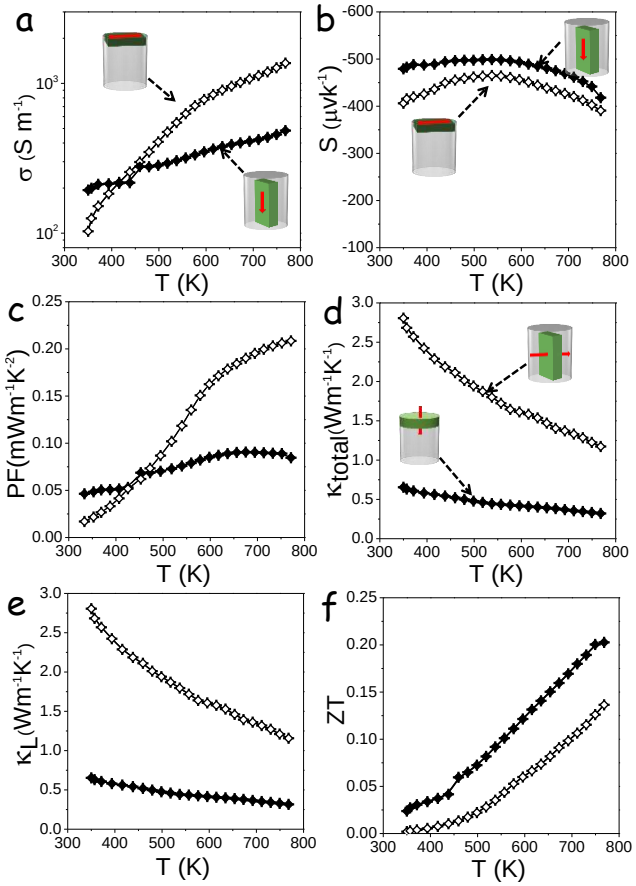

Figure 5. Temperature dependence of (a) electric conductivity, σ; (b) Seebeck coefficient, S; (c) power factor or S^2 σ, PF; (d) total thermal conductivity, κ_{total}; (e) lattice thermal conductivity, κ_L; and (f) TE figure of merit, ZT of a $SnSe_2$ pellet measured in the two directions, in-plane (//, open symbols ✧) and cross-plane (⊥, solid symbols ✦).

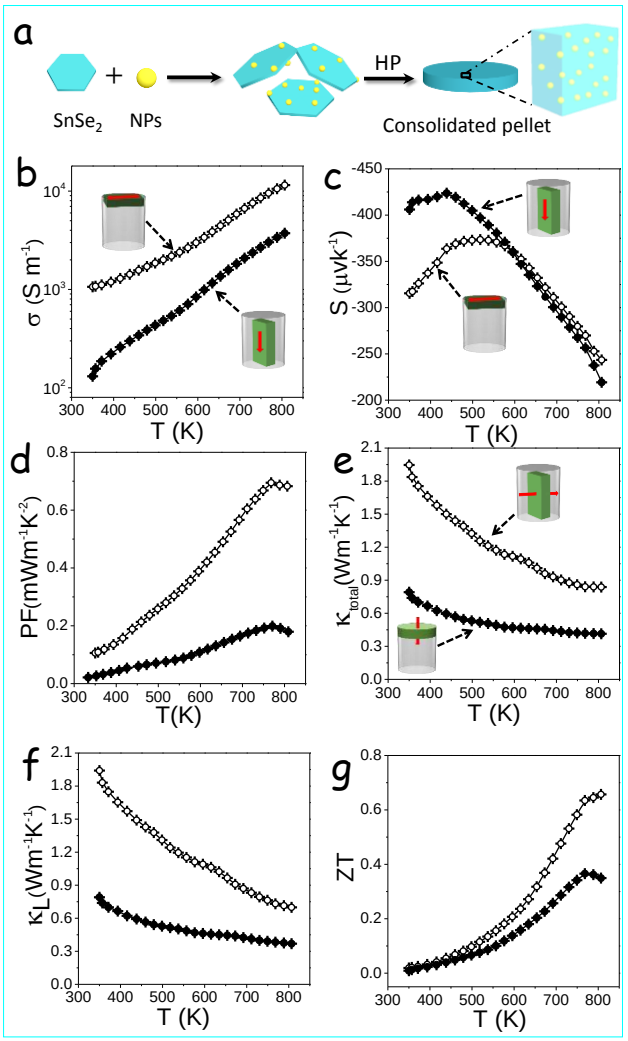

Figure 6. (a) Scheme of the process to produce $SnSe_2$-NPs nanocomposites. Thermoelectric characterization of $SnSe_2$-Cu (1.5 at%) nanocomposites. Temperature dependence of (b) electric conductivity, σ; (c) Seebeck coefficient, S; (d) power factor, PF; (e) total thermal conductivity, κ_{total}; (f) lattice thermal conductivity, κ_L; and (g) TE figure of merit, ZT. In plane (open symbols ✧); cross-plane (solid symbols ✦).

introduction of a 2.2 at% of Cu, a decrease in electrical conductivity was observed, which we associated to the formation of significant amounts of Cu_2Se, as observed by XRD characterization (Figure S8). An optimal concentration of 1.5 at% Cu was finally established to maximize TE properties of the material.

Figure 6 displays the TE properties measured in the two normal directions of the $SnSe_2$-Cu nanocomposite containing 1.5 at% of Cu. A large increase of electric conductivity and a moderate decrease of the Seebeck coefficient were observed with the Cu introduction in both directions. This translated into significantly larger power factors in the $SnSe_2$-Cu nanocomposite when compared with pure $SnSe_2$. The thermal conductivity of $SnSe_2$-Cu was significantly reduced in plane with respect to $SnSe_2$, due to the additional scattering at Cu nanoinclusions, but maintained cross plane at the already very low values measured from the $SnSe_2$ nanomaterial. Overall, a three-fold increase of the TE figure of merit was obtained with the incorporation of Cu, reaching ZT values up to ZT=0.65 at 810 K along the in plane directions.

In conclusion, we presented a solution-based approach to produce $SnSe_2$ NPLs and crystallographically textured $SnSe_2$ bulk nanomaterials and nanocomposites. The precursor solution was prepared by directly dissolving Sn and Se powders in an amine-thiol co-solvent solution. Uniform and pure phase $SnSe_2$ NPLs could be readily obtained by the crystallization of the ink at 380 °C. The growth of these $SnSe_2$ NPLs took place through a screw dislocation mechanism and the simultaneous detachment of the newly forming layers from the previously formed ones. The TE properties of thus obtained crystallographically textured $SnSe_2$ bulk nanomaterials and $SnSe_2$-Cu nanocomposites were measured in two perpendicular directions, along the press axis (cross-plane) and normal to it (in plane). While bare $SnSe_2$ nanomaterials displayed notable TE figures of merit, especially cross plane, their relatively low electrical conductivity limited their performance. A modulation doping strategy was used to improve this parameter, to reach TE figures of merit up to ZT = 0.65 at 810 K in in plane $SnSe_2$-Cu nanocomposites.

Acknowledgements

This work was supported by the European Regional Development Funds. Y.L., T.Z. and Y.Z. thank the China Scholarship Council for scholarship support. T.Z., PY. T. and J.A. acknowledge funding from Generalitat de Catalunya 2017 SGR 327 and the Spanish MINECO coordinated project VALPEC (ENE2017-85087-C3). ICN2 acknowledges support from the Severo Ochoa Programme (MINECO, Grant no. SEV-2013-0295) and is funded by the CERCA Programme / Generalitat de Catalunya. J.L. is a Serra Húnter Fellow and is grateful to ICREA Academia program and GC 2017 SGR 128.

Keywords: crystallographic texture • modulation doping • thermoelectricity • phase control • nanoplates

[1] a) D. H. Webber, R. L. Brutchey, *Journal of the American Chemical Society* 2013, *135*, 15722-15725; b) P. D. Antunez, D. A. Torelli, F. Yang, F. A. Rabuffetti, N. S. Lewis, R. L. Brutchey, *Chemistry of Materials* 2014, *26*, 5444-5446; c) C. L. McCarthy, D. H. Webber, E. C. Schueller, R. L. Brutchey, *Angewandte Chemie International Edition* 2015, *54*, 8378-8381; d) D. H. Webber, J. J. Buckley, P. D. Antunez, R. L. Brutchey, *Chemical Science* 2014, *5*, 2498-2502; e) R. Zhang, S. Cho, D. G. Lim, X. Hu, E. A. Stach, C. A. Handwerker, R. Agrawal, *Chemical Communications* 2016, *52*, 5007-5010; f) Z. Lin, C. Hollar, J. S. Kang, A. Yin, Y. Wang, H. Y. Shiu, Y. Huang, Y. Hu, Y. Zhang, X. Duan, *Advanced Materials* 2017, *29*, 1606662.

[2] D. Voiry, M. Salehi, R. Silva, T. Fujita, M. Chen, T. Asefa, V. B. Shenoy, G. Eda, M. Chhowalla, *Nano letters* **2013**, *13*, 6222-6227.

[3] a) G. Fiori, F. Bonaccorso, G. Iannaccone, T. Palacios, D. Neumaier, A. Seabaugh, S. K. Banerjee, L. Colombo, *Nature nanotechnology* **2014**, *9*, 768-779; b) D. Akinwande, N. Petrone, J. Hone, *Nature communications* **2014**, *5*, 5678.

[4] C. Lu, Y. Liu, Y. Ying, J. Liu, *Langmuir* **2017**, *33*, 630-637.

[5] L.-D. Zhao, S.-H. Lo, Y. Zhang, H. Sun, G. Tan, C. Uher, C. Wolverton, V. P. Dravid, M. G. Kanatzidis, *Nature* **2014**, *508*, 373-377.

[6] a) S. Saha, A. Banik, K. Biswas, *Chemistry–A European Journal* **2016**, *22*, 15634-15638; b) P. Xu, T. Fu, J. Xin, Y. Liu, P. Ying, X. Zhao, H. Pan, T. Zhu, *Science Bulletin* **2017**, *62*, 1663-1668; c) Y. Luo, Y. Zheng, Z. Luo, S. Hao, C. Du, Q. Liang, Z. Li, K. A. Khor, K. Hippalgaonkar, J. Xu, Q. Yan, C. Wolverton, M. G. Kanatzidis, *Advanced Energy Materials* **2018**, *8*, 1702167.

[7] a) S. J. Patil, V. C. Lokhande, D.-W. Lee, C. D. Lokhande, *Optical Materials* **2016**, *58*, 418-425; b) N. D. Boscher, C. J. Carmalt, R. G. Palgrave, I. P. Parkin, *Thin Solid Films* **2008**, *516*, 4750-4757; c) E. P. Mukhokosi, S. B. Krupanidhi, K. K. Nanda, *Scientific Reports* **2017**, *7*, 15215.

[8] a) W.-K. Burton, N. Cabrera, F. Frank, *Phil. Trans. R. Soc. Lond. A* **1951**, *243*, 299-358; b) F. Wang, X. Wang, *Nanoscale* **2014**, *6*, 6398-6414.

[9] a) L. Chen, B. Liu, A. N. Abbas, Y. Ma, X. Fang, Y. Liu, C. Zhou, *ACS nano* **2014**, *8*, 11543-11551; b) F. Meng, S. A. Morin, A. Forticaux, S. Jin, *Accounts of chemical research* **2013**, *46*, 1616-1626; c) A. Forticaux, L. Dang, H. Liang, S. Jin, *Nano letters* **2015**, *15*, 3403-3409; d) S. A. Morin, M. J. Bierman, J. Tong, S. Jin, *Science* **2010**, *328*, 476-480; e) A. Zhuang, J. J. Li, Y. C. Wang, X. Wen, Y. Lin, B. Xiang, X. Wang, J. Zeng, *Angewandte Chemie International Edition* **2014**, *53*, 6425-6429.

[10] S. A. Morin, A. Forticaux, M. J. Bierman, S. Jin, *Nano letters* **2011**, *11*, 4449-4455.

[11] a) Y. Liu, Y. Zhang, K. H. Lim, M. Ibáñez, S. Ortega, M. Li, J. David, S. Martí-Sànchez, K. M. Ng, J. Arbiol, *ACS nano* **2018,** *12*, 7174–7184 ; b) Y. Liu, Y. Zhang, S. Ortega, M. Ibáñez, K. H. Lim, A. Grau-Carbonell, S. Martí-Sánchez, K. M. Ng, J. Arbiol, M. V. Kovalenko, *Nano letters* **2018**, *18*, 2557-2563.

[12] B.-Z. Sun, Z. Ma, C. He, K. Wu, *Physical Chemistry Chemical Physics* **2015**, *17*, 29844-29853.

[13] a) M. Zebarjadi, G. Joshi, G. Zhu, B. Yu, A. Minnich, Y. Lan, X. Wang, M. Dresselhaus, Z. Ren, G. Chen, *Nano Lett* **2011**, *11*, 2225-2230; b) B. Yu, M. Zebarjadi, H. Wang, K. Lukas, H. Wang, D. Wang, C. Opeil, M. Dresselhaus, G. Chen, Z. Ren, *Nano Lett* **2012**, *12*, 2077-2082.

[14] a) M. Ibanez, Z. Luo, A. Genc, L. Piveteau, S. Ortega, D. Cadavid, O. Dobrozhan, Y. Liu, M. Nachtegaal, M. Zebarjadi, J. Arbiol, M. V. Kovalenko, A. Cabot, *Nat Commun* **2016**, *7*, 10766; b) S. Ortega, M. Ibanez, Y. Liu, Y. Zhang, M. V. Kovalenko, D. Cadavid, A. Cabot, *Chem Soc Rev* **2017**, *46*, 3510-3528; c) Y. Liu, D. Cadavid, M. Ibáñez, S. Ortega, S. M. Sánchez, O. Dobrozhan, M. V. Kovalenko, J. Arbiol, A. Cabot, *APL Materials* **2016**, 4, 104813.

Entry for the Table of Contents (Please choose one layout)

COMMUNICATION

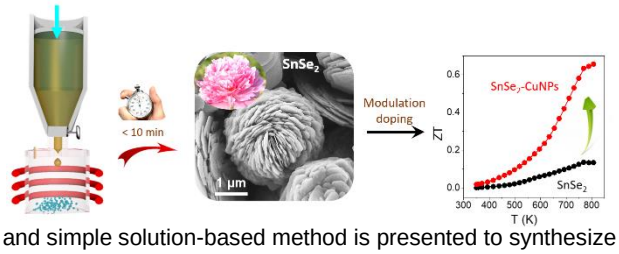

A fast and simple solution-based method is presented to synthesize flower-like $SnSe_2$ nanoplates and their use to produce crystallographically textured nanomaterials which display highly anisotropic charge and heat transport properties. Unprecedented thermoelectric performance of $SnSe_2$ is achieved through modulation doping by combining $SnSe_2$ nanoplates with metal nanoparticles.

Yu Zhang, Yu Liu, Khak Ho Lim, Congcong Xing, Mengyao Li, Ting Zhang, Pengyi Tang, Jordi Arbiol, Jordi Llorca, Ka Ming Ng, Maria Ibañez, Doris Cadavid and Andreu Cabot**

Page No. – Page No.

Tin Diselenide Molecular Precursor for Solution-Processable Thermoelectric Materials